Int. J. Solids Structures, 1970, Vol. 6, pp. 157 to 181. Pergamon Press. Printed in Great Britain

ANALYSIS OF BUCKLING AND VIBRATION OF RING-STIFFENED, SEGMENTED SHELLS OF REVOLUTION†

DAVID BUSHNELL‡

Lockheed Missiles and Space Company, Palo Alto, California

Abstract—An energy formulation is used in conjunction with the method of finite differences to develop equations leading to buckling loads and vibration frequencies of segmented elastic shells of revolution supported by rings which are treated as discrete elastic structures. A quadratic form for the total potential and kinetic energy is derived through extensive use of matrix methods. The development is similar to that used in the finite element method, and is ideally suited for programming on the digital computer. Numerical results are presented in which two types of finite difference approximations are compared, and convergence properties of eigenvalues and eigenvectors are explored.

NOTATION

A	Beginning of shell meridian
A	Ring cross-section area
B	End of shell meridian
$[B_{i1}], [B_{i2}]$	Equation (14), equation (15)
$[C]$	Constitutive equation coefficients, equation (5)
$[d]$	Displacement vector, equation (4e)
d_1, d_2	Figure 1(a)
$[D_i]$	Equation (17)
E	Young's modulus
$[E_1], [E_2]$	Equation (23), equation (24)
e_1, e_2	Figure 1(a)
$[F]$	Equation (42)
G	Shear modulus
$[G_1], [G_2]$	Equation (20), equation (21)
H_n	Hamiltonian corresponding to n-wave pattern
h	Finite difference mesh spacing
I	Ring moment of inertia (subscripted)
J	Ring torsion constant
K	Number of shell segments in shell structure
$[K_1], [K_2]$	Stiffness matrices, equations (2), (45) and (46)
$[K^m]$	Equations (38) and (39)
$K_{A1}, K_{A2}, \ldots$	Boundary condition designators for A end of shell meridian
$K_{B1}, K_{B2}, \ldots$	Boundary condition designators for B end of shell meridian
m	Shell mass/area
$[M]$	Mass matrix, equation (47)
M	Total number of rings
M	Bending moment resultants (subscripted)
n	Number of circumferential waves in buckling or vibration mode
N	Total number of stations at which H_n is evaluated (e.g. 13 in Fig. 1(b))

† The development of the computer program based on the theory described herein was sponsored by the Structural Mechanics Laboratory of the Naval Ship Research and Development Center under Contract N00014-67-C-0256, NAVSHIPS Subproject ZF 013 01 01.

‡ Staff Scientist, Aerospace Sciences Laboratory.

N	In-plane stress resultants (subscripted)
$[N_o]$	Prestress matrix, equation (4d)
$[P]$	Equation (4f)
p	Normal pressure
$\lfloor q \rfloor$	Displacement vector, equation (10)
$[Q_1], [Q_2]$	Equation (35), equation (36)
r	Parallel circle radius, Fig. 1(a)
R	Radius of curvature (subscripted), Fig. 1(a)
$[R]$	Equation (16)
s	Arc length measured from point A
Δs_i	Weighting factor for numerical integration
$\lfloor S \rfloor$	Stress vector, equation (4a)
t	Shell thickness
$[T]$	Equation (26)
T_s, T_r	Kinetic energy of shell, ring
u, u^*	Meridional, axial displacement, Fig. 1(a)
U_s, U_r	Strain energy of shell, ring
U_c	Constraint "energy"
v, v^*	Circumferential displacement
$\bar{V}$	Axial load applied to ring centroid
w, w^*	Normal, radial displacement, Fig. 1(a)
α	Spherical shell edge angle
γ	Rotation around normal, equation (8c)
δ_i^j	Kronecker delta: $\delta_i^j = 1$ if $i = j$; 0 otherwise
$\lfloor \varepsilon \rfloor$	Strain vector, equations 4(b), (6) and (7)
λ_i^m	Lagrange multipliers for constraint conditions
λ	Eigenvalue
$\varkappa$	Changes in curvature, equation (7)
$\lfloor \omega \rfloor$	Rotation vector, equations (4c) and (8)
Ω	Eigenfrequency
ψ	Rotation about meridian, equation (8b)
χ	Rotation of meridian, equation (8a)
θ	Circumferential coordinate
ν	Poisson's ratio

Subscripts

c	Ring centroid
cr	Critical
i	ith mesh point
j	Mesh point corresponding to ring attachment point
l	Mesh point corresponding to $(\ )^-$ side of juncture
n	Circumferential wave number, also with respect to axis Normal to shell meridian (Fig. 1(a))
o	Prebuckling quantity
p	Polar
r	Ring quantity
s	Shell, shear center, or with respect to axis parallel to shell meridian (Fig. 1(a))
t	Twist; $M_t = (M_{12} + M_{21})/2$
x, y, xy	With respect to x–y system (Fig. 1(a))
O	Prebuckling quantity
1, 2	Meridional, circumferential directions
12	Shear

Superscripts

k	kth ring support
m	mth set of constraints
T	Transpose
$+, -$	Figure 1(a)
$(\ )'$	Differentiation with respect to s
*	Figure 1(a)

INTRODUCTION

RECENT investigations have taken advantage of larger and faster computers to analyze more accurate models of shell structures. Cohen [1], [2] uses a step-by-step numerical integration technique to calculate buckling loads and vibration frequencies of ring-stiffened orthotropic shells of revolution. Kalnins [3] employs a similar method to calculate nonsymmetric deformations of segmented shells of revolution submitted to nonsymmetric loads. In [4] a computer program is described by which buckling loads are calculated for axisymmetrically loaded shells of revolution with general wall construction and with ring supports at the edges.

In this paper the finite difference method is used for the analysis of shells of revolution consisting of elastic shell segments joined by elastic rings. The shell segments may be of various geometries and wall constructions. There are two parts of the analysis: a part in which the axisymmetric state of an axisymmetrically loaded shell is calculated from nonlinear theory, and a part in which buckling loads and natural frequencies corresponding to nonsymmetric displacements are calculated. Equilibrium equations similar to those derived by Reissner [5] are used for the prebuckling analysis, and an energy method based on kinematic relations given by Novoshilov [6] is used for the buckling and vibration analysis. The assumptions governing the analysis are:

1. The material is linear–elastic.
2. The Kirchhoff–Love hypothesis holds: normals to the undeformed surface remain unstrained and normal to the deformed middle surface.
3. The structure and loads are axisymmetric, and the prebuckling or prestress deformations are axisymmetric.
4. The prebuckling deflections, while considered finite, are moderate. That is, the square of the meridional rotation can be neglected compared to unity.
5. The ring stiffeners are reasonably "thin". That is, a typical cross-section dimension is small compared to the radius of the ring.
6. The cross-sections of the rings remain undeformed during the deformations of the structure, and the rotation about the ring centroid is equal to the rotation of the shell meridian at the attachment point of the ring.
7. The ring centroids coincide with the ring shear centers.
8. If meridional stiffeners are present, they are numerous enough to include in the analysis by an averaging or "smearing" of their properties over any parallel circle of the shell structure.

For axisymmetrically loaded shells of revolution the partial differential equations governing nonsymmetric buckling and vibration can be reduced to ordinary differential equations through separation of variables. These equations can be solved by application of numerical integration, finite difference, or finite element techniques. With the existence of large computers it is now practical to solve with reasonable accuracy almost any buckling or vibration problem for shells of revolution. It is, for instance, easy to include in the buckling or vibration equations prebuckling quantities as they are obtained from a nonlinear analysis. While nonlinear equations were used for instance by Weinitschke [7] and Budiansky [8] for the symmetrical snapping of spherical caps, the influence of the prebuckling displacements and stresses on bifurcation buckling was first recognized by Stein [9] for cylindrical shells and by Huang [10] for spherical caps. In cases such as that treated by

Stuhlman *et al.* in [11] with edge moments introducing hoop stresses in the shell, it is imperative that an accurate prebuckling analysis be used.

This paper contains the buckling and vibration analysis only. The nonlinear prebuckling analysis for the axisymmetric prestress is given in [12], in the following it is assumed that this prestress state is known. Some numerical results are given in which two finite-difference schemes are compared, convergence properties are demonstrated, and the effects of round-off errors are revealed. Further numerical results are given in a separate paper [13] in which several comparisons are made between theory and experiment for the buckling of various shells of revolution. Some natural frequencies of an axially compressed, ring and stringer-stiffened cylinder are also given in [13].

It is felt that the major contribution of this paper is the derivation of a practical approach to the solution of a wide class of problems which confront the designer of complex shell structures. The development is similar to that used in the finite element method, and is ideally suited for programming on the digital computer.

The numerical results in this paper and in [12] and [13] were obtained by means of a digital computer code called Bosor 2, which is based on the analyses presented here and in [12]. The Bosor 2 program has a broader capability than its predecessor the Bosor (Buckling of Shells of Revolution) program, which is based on the analysis in [4]. The extensions include:

1. Analysis of segmented (composite) shells, such as cylindercone combinations or joined shells with dissimilar wall characteristics.
2. Analysis of the free vibrations of prestressed, segmented, ring-stiffened shells of revolution.
3. Analysis of shells with discrete rings at a number of stations along the meridian, rather than at the boundaries only.
4. Use of more accurate kinematic relations. The analysis of [4] is based on Donnell-type equations. The analysis which follows is based on Novoshilov-type kinematic relations.
5. Analysis of shells with wall properties which vary along the meridian.
6. Increased generality of the type of axisymmetric loading applied to the shell.

One of the more important extensions of the analysis of [4] is the capability of treating segmented shells. This capability can also be used to advantage in the analysis of simple shells. For instance a rather long cylinder submitted to pressure loading can be divided artificially into three segments: two edge segments in which stresses and displacements vary rapidly over short lengths, and a central segment in which deformations are uniform. The station spacing in the finite difference mesh can be small in the two edge segments and large in the central segment. It has been found from experience that it is better to divide the shell into segments, and thus to maintain uniform station spacing within each segment, rather than to vary the station spacing within any segment.

ANALYSIS FOR BUCKLING AND VIBRATION

The nonlinear analysis for the axisymmetric prestress is given in [12]. In the present paper it is assumed that this prestress state is known. The quantities N_{10}, N_{20}, N_{or}, and χ_0 appear in the buckling and vibration analyses as known variable coefficients.

The energy method used in the eigenvalue analysis is based on the definition of the Hamiltonian corresponding to an n-wave deformation pattern:

$$H_n = U_s + \sum_{k=1}^{M} U_r^k - \left(T_s + \sum_{k=1}^{M} T_r^k \right) + \sum_{i=1}^{K+1} U_c^i \tag{1}$$

where

U_s = shell strain energy
U_r^k = strain energy of kth ring stiffener
T_s = shell kinetic energy
T_r^k = kinetic energy of kth ring stiffener
U_c^i = ith set of constraint conditions.

The functional H_n is given in terms of the shell wall displacements and their derivatives. Integration along the shell meridian is performed numerically. The derivatives with respect to the meridional coordinate "s" are simulated by two and three point finite-difference formulas. The derivatives with respect to the circumferential coordinate θ are eliminated because $U = u_n \sin n\theta$, $V = v_n \cos n\theta$, $W = w_n \sin n\theta$. In this way H_n, which is originally an integro-differential quadratic form, becomes an algebraic quadratic form. The constraint conditions are equations of displacement and rotation compatibility at junctures between shell segments and at the shell boundaries.

The algebraic quadratic form H_n is expressed as:

$$H_n = \lfloor q \rfloor [[K_1] + [K_2] + \Omega^2 [M]] \{q\}. \tag{2}$$

The vector $\lfloor q \rfloor$ represents the dependent variables. These include the displacements at the meridional stations in the finite difference mesh and Lagrange multipliers corresponding to the constraint conditions. The matrix $[K_1]$ represents the stiffness matrix (including constraints) of the undeformed and unstressed structure; $[K_2]$ represents the contribution of the prestress terms N_{10}, N_{20}, N_{or}, and χ_0 to the stiffness matrix; and $[M]$ represents the mass matrix. These matrices are symmetric.

The problem is to find the value (eigenvalue) of a parameter which causes H_n to be an extremum. In vibration problems the eigenvalue parameter is the square of the frequency Ω^2. In buckling problems the eigenvalue parameter may be the pressure amplitude p, or any line load or moment $\bar{V}$, $\bar{H}$ or $\bar{M}$ applied to any ring. If some applied load is regarded as the eigenvalue parameter, the kinetic energy terms T_s and T_r^k are zero. The lowest eigenvalue then represents the bifurcation load and the eigenvector represents the mode shape. If, however, the applied load is fixed and Ω^2 is regarded as the eigenvalue parameter, the terms T_s and T_r^k are non-zero. The eigenvalues and eigenvectors then represent frequencies and mode shapes for prestressed shells of revolution. Minimization of H_n with respect to all of the q-components generates a set of simultaneous linear homogeneous algebraic equations, the coefficient matrix of which is symmetric. Nontrivial solutions are obtained for these equations on the digital computer.

Derivation of $[K_1]$, $[K_2]$, *and* $[M]$

In the following derivation variables are used which are defined in Figs. 1(a) and 1(b). These figures show a segmented, ring-stiffened shell supported at the end A by a ring and clamped at B. There are two intermediate rings, one in segment $\#1$ and one between

segments #1 and #2. Fig. 1(a) shows the structure and Fig. 1(b) shows the corresponding finite-difference model.

It is necessary first to define the various components of strain energy and kinetic energy. The shell strain energy U_s can be written as:

$$U_s = \frac{\pi}{2}\int_A^B [\lfloor S\rfloor\{\varepsilon\} + \lfloor\omega\rfloor[N_0]\{\omega\} + \lfloor d\rfloor[P]\{d\}]r\,ds \tag{3}$$

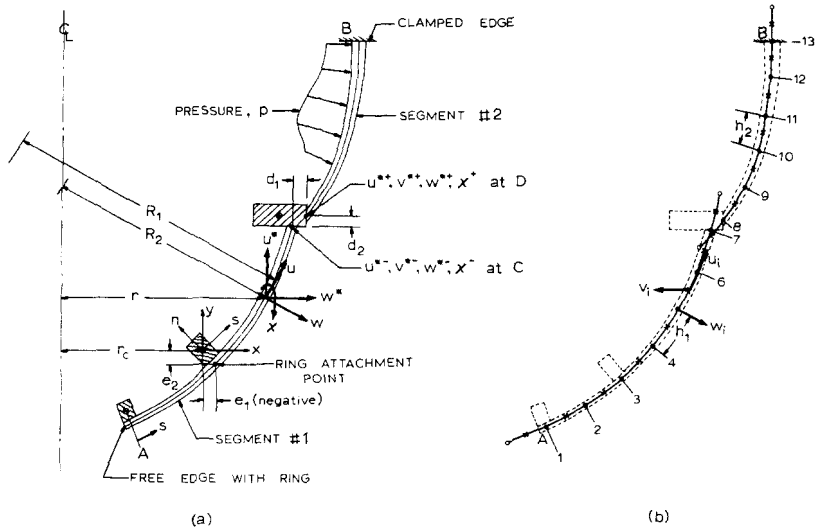

FIG. 1. Ring-stiffened shell with two segments.

where

$$\lfloor S\rfloor \equiv \lfloor N_1, N_2, N_{12}, M_1, M_2, M_t\rfloor$$

$$\lfloor\varepsilon\rfloor \equiv \{\varepsilon\}^T \equiv \lfloor\varepsilon_1, \varepsilon_2, \varepsilon_{12}, \varkappa_1, \varkappa_2, 2\varkappa_{12}\rfloor$$

$$\lfloor\omega\rfloor \equiv \lfloor\chi, \psi, \gamma\rfloor$$

$$[N_0] = \begin{bmatrix} N_{10} & 0 & 0 \\ 0 & N_{20} & 0 \\ 0 & 0 & (N_{10}+N_{20}) \end{bmatrix} \tag{4}$$

$$\lfloor d\rfloor \equiv \lfloor u, v, w\rfloor$$

$$[P] = \begin{bmatrix} -p/R_1 & 0 & -p' \\ 0 & -p/R_2 & 0 \\ -p' & 0 & p(1/R_1+1/R_2) \end{bmatrix}$$

and

$$\begin{Bmatrix} N_1 \\ N_2 \\ N_{12} \\ M_1 \\ M_2 \\ M_t \end{Bmatrix} = [C]\{\varepsilon\} = \begin{bmatrix} C_{11} & C_{12} & 0 & C_{14} & C_{15} & 0 \\ C_{12} & C_{22} & 0 & C_{24} & C_{25} & 0 \\ 0 & 0 & C_{33} & 0 & 0 & C_{36} \\ C_{14} & C_{24} & 0 & C_{44} & C_{45} & 0 \\ C_{15} & C_{25} & 0 & C_{45} & C_{55} & 0 \\ 0 & 0 & C_{36} & 0 & 0 & C_{66} \end{bmatrix} \begin{Bmatrix} \varepsilon_1 \\ \varepsilon_2 \\ \varepsilon_{12} \\ \varkappa_1 \\ \varkappa_2 \\ 2\varkappa_{12} \end{Bmatrix} \tag{5}$$

$$\begin{aligned} \varepsilon_1 &= u' + w/R_1 + \chi_0\chi \\ \varepsilon_2 &= -nv/r + r'u/r + w/R_2 \\ \varepsilon_{12} &= v' - r'v/r + nu/r + \chi_0\psi \end{aligned} \tag{6}$$

$$\begin{aligned} \varkappa_1 &= \chi' \\ \varkappa_2 &= -n\psi/r + r'\chi/r \\ 2\varkappa_{12} &= 2(-n\chi/r + r'\psi/r + v'/R_2) \end{aligned} \tag{7}$$

$$\begin{aligned} \chi &= w' - u/R_1 \\ \psi &= nw/r - v/R_2 \\ \gamma &= \tfrac{1}{2}(nu/r - rv'/r - r'v/r). \end{aligned} \tag{8}$$

The first term in the integrand of equation (3) is contained in equation (3) of [2]; the second term appears in equation (2) of [14]; and the third term appears in equation (9) of [15]. The coefficients C_{ij} of the constitutive equations (5) are given for various types of shell walls (eccentrically stiffened, layered orthotropic, fiber-wound, corrugated) in [16]. The values of C_{36} and C_{66} in the present analysis are equal to one-half the values given in [16] because of the multiplier 2 in the column vector component $2\varkappa_{12}$. The kinematic relations (6)–(8) which relate infinitesimal buckling strains, changes in curvature, and rotations to infinitesimal buckling displacements are given in equations (4.23) and equations (3.16) of [6] and Equations (7) and (12) of [2].

Figure 1(b) shows the shell meridian with stations $1, 2, 3, 4, \ldots, 13$ identified. The Hamiltonian H_n is expressed at these stations in terms of the displacement components u_i, v_i, and w_i, and the integration in equation (3) is replaced by summation over all stations. The tangential displacement components u_i and v_i occur at stations midway between the stations for w_i and w_{i+1}. A similar arrangement of mesh points was used by Stein in [9]. At the ends of each segment there are "fictitious" points, shown as circles, which correspond to w-values. These points are needed for the expression of the first and second derivatives of w with respect to s at the ends of the segments. The arrangement of mesh points and displacements shown in Fig. 1(b) has been determined to be superior to an arrangement in which u_i, v_i and w_i correspond to displacement components at a single point. More will be said about this in the section on Numerical Results. The station spacing in each segment is constant, but different spacings are used in different segments ($h_1 \neq h_2$

in Fig. 1(b)). The displacements and their derivatives at the ith station are:

$$\begin{aligned} u &= (u_i+u_{i-1})/2 \qquad v = (v_i+v_{i-1})/2 \qquad w = w_i, \\ u' &= (u_i-u_{i-1})/h \qquad v' = (v_i-v_{i-1})/h \qquad w' = (w_{i+1}-w_{i-1})/2h, \\ w'' &= (w_{i+1}-2w_i+w_{i-1})/h^2. \end{aligned} \tag{9}$$

It is convenient to define the vector $\lfloor q_i \rfloor$ by

$$\lfloor q_i \rfloor \equiv \{q_i\}^T \equiv \lfloor w_{i-1}, u_{i-1}, v_{i-1}, w_i, u_i, v_i, w_{i+1} \rfloor. \tag{10}$$

From equations (6)–(10) it follows that

$$\{\varepsilon_i\} = [[B_{i1}]+\chi_{oi}[B_{i2}]]\{q_i\} \tag{11}$$

$$\{\omega_i\} = [R_i]\{q_i\} \tag{12}$$

$$\{d\} = [D_i]\{q_i\} \tag{13}$$

in which

$$[B_{i1}] \equiv \begin{bmatrix} 0 & -1/h & 0 & 1/R_1 \\ 0 & r'/2r & -n/2r & 1/R_2 \\ 0 & n/2r & \left(-\frac{1}{h}-\frac{r'}{2r}\right) & 0 \\ \frac{1}{h^2} & \left[\frac{1}{hR_1}-\frac{(1/R_1)'}{2}\right] & 0 & -\frac{2}{h^2} \\ -r'/2rh & -r'/2rR_1 & n/2rR_2 & -n^2/r^2 \\ \frac{n}{rh} & \frac{n}{rR_1} & \left(-\frac{r'}{rR_2}-\frac{2}{hR_2}\right) & 2\frac{nr'}{r^2} \end{bmatrix}$$

$$\begin{bmatrix} 1/h & 0 & 0 \\ r'/2r & -n/2r & 0 \\ n/2r & \left(\frac{1}{h}-\frac{r'}{2r}\right) & 0 \\ \left[-\frac{1}{hR_1}-\frac{(1/R_1)'}{2}\right] & 0 & \frac{1}{h^2} \\ -r'/2rR_1 & n/2rR_2 & r'/2rh \\ \frac{n}{rR_1} & \left(-\frac{r'}{rR_2}+\frac{2}{hR_2}\right) & -\frac{n}{rh} \end{bmatrix} \tag{14}$$

$$[B_{i2}] \equiv \begin{bmatrix} -1/2h & -1/2R_1 & 0 & 0 & -1/2R_1 & 0 & 1/2h \\ 0 & 0 & 0 & 0 & 0 & 0 & 0 \\ 0 & 0 & -1/2R_2 & n/r & 0 & -1/2R_2 & 0 \\ 0 & 0 & 0 & 0 & 0 & 0 & 0 \\ 0 & 0 & 0 & 0 & 0 & 0 & 0 \\ 0 & 0 & 0 & 0 & 0 & 0 & 0 \end{bmatrix} \tag{15}$$

$$[R_i] \equiv \begin{bmatrix} -1/2h & -1/2R_1 & 0 & 0 & -1/2R_1 & 0 & 1/2h \\ 0 & 0 & -1/2R_2 & n/r & 0 & -1/2R_2 & 0 \\ 0 & n/4r & \left(\frac{1}{2h}-\frac{r'}{4r}\right) & 0 & n/4r & \left(-\frac{1}{2h}-\frac{r'}{4r}\right) & 0 \end{bmatrix} \tag{16}$$

$$[D_i] = \begin{bmatrix} 0 & 1/2 & 0 & 0 & 1/2 & 0 & 0 \\ 0 & 0 & 1/2 & 0 & 0 & 1/2 & 0 \\ 0 & 0 & 0 & 1 & 0 & 0 & 0 \end{bmatrix}. \tag{17}$$

For convenience the subscript i has been omitted from the arrays in equations (14)–(16). The geometrical parameters r, r', $1/R_1$, $1/R_2$ and $(1/R_1)'$ are evaluated at every station. The station spacing h should also be subscripted, since it varies from segment to segment.

Insertion of equations (5) and (11)–(16) into equation (3), and replacement of the integral with summation over the number of stations in the finite-difference mesh leads to

$$\begin{aligned} U_s = \frac{\pi}{2} \sum_{i=1}^{N} r_i \Delta s_i [q_i][[[B_{i1}]^T + \chi_{oi}[B_{i2}]^T][C_i][[B_{i1}] + \chi_{oi}[B_{i2}]] \\ + [R_i]^T[N_{oi}][R_i] + [D_i]^T[P_i][D_i]]\{q_i\}. \end{aligned} \tag{18}$$

The integration weights Δs_i are equal to h for all stations except the end stations of each segment, at which $\Delta s_i = h/2$. The strain energy of the kth ring stiffener can be written in the form

$$U_r^k = \frac{\pi}{2} r_c^k [u_s^*, v_s^*, w_s^*, \chi]^k [G_1^k + G_2^k] \begin{Bmatrix} u_s^* \\ v_s^* \\ w_s^* \\ \chi \end{Bmatrix}^k \tag{19}$$

in which r_c^k is the radius to the centroid of the kth ring and u_s^*, v_s^*, and w_s^* are the axial, circumferential, and radial displacements of the ring shear center. (In this paper the shear center is assumed to coincide with the centroid.) The quantity G_1 is the stiffness matrix of

the unstressed ring, given from [1] by

$$[G_1^k] = \frac{E}{r_c^2}\begin{bmatrix} n^2(n^2I_x+GJ/E)/r_c^2 & -n^3I_{xy}/r_c^2 & n^4I_{xy}/r_c^2 & n^2(I_x+GJ/E)/r_c \\ & n^2(A+I_y/r_c^2) & -n(A+n^2I_y/r_c^2) & -nI_{xy}/r_c \\ & & A+n^4I_y/r_c^2 & n^2I_{xy}/r_c \\ \text{Symmetric} & & & I_x+n^2GJ/E \end{bmatrix} \tag{20}$$

and G_2^k represents the effect of prestress on the ring stiffness:

$$[G_2^k] = \frac{N_{or}}{r_c^2}\begin{bmatrix} n^2 & 0 & 0 & 0 \\ & 1 & -n & 0 \\ & & n^2 & 0 \\ \text{Symmetric} & & & 0 \end{bmatrix}. \tag{21}$$

The displacements and the rotation of the ring shear center during buckling are related to those of the point on the shell reference surface which corresponds to the attachment point of the ring (see Fig. 1(a)) by

$$\begin{Bmatrix} u_s^* \\ v_s^* \\ w_s^* \\ \chi \end{Bmatrix}^k = [E_i^k + \chi_{oj}^k E_2^k]\begin{Bmatrix} u^* \\ v^* \\ w^* \\ \chi \end{Bmatrix}_j \tag{22}$$

in which $[E_1^k]$ is the transformation matrix for the undeformed shell, given by

$$[E_1^k] = \begin{bmatrix} 1 & 0 & 0 & -e_1 \\ -e_2n/r & (1+e_1/r) & -e_1n/r & 0 \\ 0 & 0 & 1 & e_2 \\ 0 & 0 & 0 & 1 \end{bmatrix} \tag{23}$$

and $[E_2^k]$ represents the effect of "prebuckling" meridional rotation on the transformation (22):

$$[E_2^k] = \begin{bmatrix} 0 & 0 & 0 & -e_2 \\ e_1n/r & e_2/r & -e_2n/r & 0 \\ 0 & 0 & 0 & -e_1 \\ 0 & 0 & 0 & 0 \end{bmatrix}. \tag{24}$$

In equations (20)–(24) the superscript k has been omitted from the arrays. The subscript j is the meridional station number corresponding to the ring attachment point. The vector

$[u^*, v^*, w^*, \chi]_j$ is related to the vector $[q_j]$ by

$$\begin{Bmatrix} u^* \\ v^* \\ w^* \\ \chi \end{Bmatrix}_j = [T]\{q_j\} \tag{25}$$

where

$$[T] = \begin{bmatrix} 0 & r/2R_2 & 0 & -r' & r/2R_2 & 0 & 0 \\ 0 & 0 & 1/2 & 0 & 0 & 1/2 & 0 \\ 0 & r'/2 & 0 & r/R_2 & r'/2 & 0 & 0 \\ -1/2h & -1/2R_1 & 0 & 0 & -1/2R_1 & 0 & 1/2h \end{bmatrix}. \tag{26}$$

Equations (22) and (25) can be used for determination of U_r^k in equation (19) in terms of $\{q_j\}$:

$$U_r^k = \frac{\pi}{2} r_c^k [q_j][T]^T [E_1^k + \chi_{oj} E_2^k]^T [G_1^k + G_2^k][E_1^k + \chi_{oj} E_2^k][T]\{q_j\}. \tag{27}$$

The kinetic energy of the shell is given by

$$T_s = \frac{\pi}{2}\Omega^2 \int_A^B m(u^2 + v^2 + w^2) r \, ds \tag{28}$$

which, by use of equations (4e) and (13), and with numerical integration can be written in the form:

$$T_s = \frac{\pi}{2}\Omega^2 \sum_{i=1}^{N} m_i r_i \Delta s_i [q_i][D]^T [I][D]\{q_i\}. \tag{29}$$

The quantity m_i represents the mass/area at the ith station and $[I]$ is the identity matrix. The kinetic energy of the kth ring is given by

$$T_r^k = \frac{\pi}{2}\Omega^2 \rho_r^k r_c^k [A^k (u_{cj}^{*2} + v_{cj}^{*2} + w_{cj}^{*2}) + I_p^k \chi_j^2 + I_s^k \psi_j^2 + I_n^k \gamma_j^2 - 2I_{sn}^k \psi_j \gamma_j]. \tag{30}$$

Subscript c denotes ring centroid and j denotes meridional station corresponding to the ring attachment point. In this work the centroid is assumed to coincide with the shear center. By use of equations (4c), (12), (22) and (25), equation (30) can be written in the form

$$T_r^k = \frac{\pi}{2}\Omega^2 \rho_r^k r_c^k [q_j][A^k [T]^T [E_1^k + \chi_{oj} E_2^k]^T [T_A^k][E_1^k + \chi_{oj} E_2^k][T] + [R]^T [T_B^k][R]]\{q_j\} \tag{31}$$

where

$$[T_A^k] = \begin{bmatrix} 1 & 0 & 0 & 0 \\ 0 & 1 & 0 & 0 \\ 0 & 0 & 1 & 0 \\ 0 & 0 & 0 & I_p^k/A^k \end{bmatrix} \tag{32}$$

and

$$[T_B^k] = \begin{bmatrix} 0 & 0 & 0 \\ 0 & I_s^k & -I_{sn}^k \\ 0 & -I_{sn}^k & I_n^k \end{bmatrix} \tag{33}$$

The mth constraint condition U_c^m can be written in the form

$$U_c^m = [\lambda_1^m, \lambda_2^m, \lambda_3^m, \lambda_4^m] \left[[I] \begin{Bmatrix} u^{*+} \\ v^{*+} \\ w^{*+} \\ \chi^+ \end{Bmatrix}_l + [Q_1^m + \chi_{0_l} Q_2^m] \begin{Bmatrix} u^{*-} \\ v^{*-} \\ w^{*-} \\ \chi^- \end{Bmatrix}_l \right] \tag{34}$$

in which subscript l refers to the meridional station corresponding to the mth juncture between segments, and $[Q_1^m]$ and $[Q_2^m]$ are analogous to the negatives of $[E_1^k]$ and $[E_2^k]$:

$$[Q_1^m] = \begin{bmatrix} -1 & 0 & 0 & d_1 \\ nd_2/r & -(1+d_1/r) & nd_1/r & 0 \\ 0 & 0 & -1 & -d_2 \\ 0 & 0 & 0 & -1 \end{bmatrix}, \tag{35}$$

$$[Q_2^m] = \begin{bmatrix} 0 & 0 & 0 & d_2 \\ -nd_1/r & -d_2/r & nd_2/r & 0 \\ 0 & 0 & 0 & d_1 \\ 0 & 0 & 0 & 0 \end{bmatrix}. \tag{36}$$

In equations (35) and (36) superscript m has been omitted for convenience from the arrays. The λ_1^m, λ_2^m, λ_3^m, and λ_4^m are the mth set of Lagrange multipliers associated with the lth station at which constraints are imposed on the quantities u^*, v^*, w^* and χ. For example, the constraint conditions between Segments #1 and #2 in Fig. 1 ($m = 2$, $l = 7$) arise from the requirement that the motion during buckling or vibration of point D relative to point C involves no deformation of the ring cross-section. The quantity λ_1^m corresponds to compatibility of axial displacements u^{*-} and u^{*+}; λ_2^m corresponds to compatibility of circumferential displacements v^{*-} and v^{*+}; λ_3^m to compatibility of radial displacements w^{*-} and w^{*+}; and λ_4^m to compatibility of meridional rotations χ^- and χ^+.

Displacement boundary conditions applied at the A and B ends of the meridian (see Fig. 1) take the form

$$U_c^m = [\lambda_1^m, \lambda_2^m, \lambda_3^m, \lambda_4^m][K^m][Q_1^m + \chi_{o_l} Q_2^m] \begin{Bmatrix} u^* \\ v^* \\ w^* \\ \chi \end{Bmatrix}_l \tag{37}$$

in which at the end A of the meridian $m = 1$ with

$$[K^m] = \begin{bmatrix} K_{A1} & 0 & 0 & 0 \\ 0 & K_{A2} & 0 & 0 \\ 0 & 0 & K_{A3} & 0 \\ 0 & 0 & 0 & K_{A4} \end{bmatrix} \tag{38}$$

and at the end B of the meridian $m = K+1$ (K = number of shell segments) with

$$[K^m] = \begin{bmatrix} K_{B1} & 0 & 0 & 0 \\ 0 & K_{B2} & 0 & 0 \\ 0 & 0 & K_{B3} & 0 \\ 0 & 0 & 0 & K_{B4} \end{bmatrix}. \tag{39}$$

The quantities K_{A1}, K_{A2}, etc. and K_{B1}, K_{B2}, etc. are assigned values, either unity if the corresponding displacement component is zero or zero if the corresponding force component is zero. The displacement conditions correspond to a shell which is supported at distances d_1^m and d_2^m from the reference surface. For the shell in Fig. 1(a) the K_{A1}, K_{A2}, etc. would all be zero and the K_{B1}, K_{B2}, etc. would all be unity. The constraint conditions (34) and (37) can be written in terms of the vectors $\lfloor q^+ \rfloor$ and $\lfloor q^- \rfloor$ by introduction of equation (25). The compatibility condition (34) can be written as a symmetric quadratic form in the following way:

$$U_c^m = \lfloor q^-, \lambda, q^+ \rfloor [F] \begin{Bmatrix} q^- \\ \lambda \\ q^+ \end{Bmatrix} \tag{40}$$

with

$$\lambda \equiv \lfloor \lambda_1^m, \lambda_2^m, \lambda_3^m, \lambda_4^m \rfloor \tag{41}$$

$$[F] = \begin{bmatrix} 7\times 7 & 7\times 4 & 7\times 7 \\ [0] & [QT]^T & [0] \\ 4\times 7 & 4\times 4 & 4\times 7 \\ [QT] & [0] & [T] \\ 7\times 7 & 7\times 4 & 7\times 7 \\ [0] & [T]^T & [0] \end{bmatrix} \tag{42}$$

$$Q \equiv [Q_1^m + \chi_{0,t} Q_2^m]. \tag{43}$$

The boundary conditions (37) take a similar form:

$$U_c^m = \lfloor q^-, \lambda, q^+ \rfloor \begin{bmatrix} [0] & [KQT]^T & [0] \\ [KQT] & [0] & [0] \\ [0] & [0] & [0] \end{bmatrix} \begin{Bmatrix} q^- \\ \lambda \\ q^+ \end{Bmatrix}. \tag{44}$$

The three coefficient matrices $[K_1]$, $[K_2]$ and $[M]$ in equation (2) can now be written through use of equations (18), (27), (29), (31), (34) and (40). The following expressions are obtained:

$$\lfloor q\rfloor[K_1]\{q\} = \frac{\pi}{2}\sum_{i=1}^{N}\left\{\lfloor q_i\rfloor[r_i\Delta s_i[B_{i1}]^T[C_i][B_{i1}]+\delta_i^j[T]^T[E_1]^T[G_1][E_1][T]]\{q_i\}\right.$$
$$\left.+\delta_i^j\lfloor q^-,\lambda,q^+\rfloor[F_1]\begin{Bmatrix}q^-\\ \lambda\\ q^+\end{Bmatrix}\right\} \tag{45}$$

$$\lfloor q\rfloor[K_2]\{q\} = \frac{\pi}{2}\sum_{i=1}^{N}\left\{\lfloor q_i\rfloor[r_i\Delta s_i(\chi_{oi}[B_{i1}]^T[C_i][B_{i2}]+\chi_{oi}[B_{i2}]^T[C_i][B_{i1}]\right.$$
$$+\chi_o^2[B_{i2}]^T[C_i][B_{i2}]+[R_i]^T[N_{oi}][R_i]+[D_i]^T[P_i][D_i])$$
$$+\delta_i^j\{[T]^T(\chi_o[E_1]^T[G_1+G_2][E_2]+\chi_o[E_2]^T[G_1+G_2][E_1] \tag{46}$$
$$\left.+\chi_o^2[E_2]^T[G_1+G_2][E_2]+[E_1]^T[G_2][E_1])[T]\}\right]\{q_i\}$$
$$\left.+\delta_i^j[q^-,\lambda,q^+][F_2]\begin{Bmatrix}q^-\\ \lambda\\ q^+\end{Bmatrix}\right\}$$

$$\lfloor q\rfloor[M]\{q\} = \frac{\pi}{2}\sum_{i=1}^{N}\lfloor q_i\rfloor[m_ir_i\Delta s_i[D]^T[I][D]$$
$$+\delta_i^j\rho_r r_c(A[T]^T[E_1+\chi_{oi}E_2]^T[T_A][E_1+\chi_{oi}E_2][T]+[R]^T[T_B][R])]\{q_i\}. \tag{47}$$

The δ_i^j and δ_i^j are Kronecker deltas, and $[F_1]$ and $[F_2]$ refer to equation (42) with the first and second parts of the matrix Q, respectively [equation (43)].

The coefficient matrices $[K_1]$, $[K_2]$ and $[M]$ have the form shown in Fig. 2. This matrix corresponds to the shell modeled as shown in Fig. 1(b). The boundary conditions at A contribute the elements $[KQT]_1$ and $[KQT]_1^T$; the compatibility conditions for conformity of displacements and rotation at the juncture between Segment #1 and Segment #2 contribute the elements $[QT]_2$, $[QT]_2^T$, $[T]$, and $[T]^T$; and the boundary conditions at B contribute the elements $[KQT]_3$ and $[KQT]_3^T$. Expression of H_n at each of the stations 1 through 13 leads to the sub-arrays of elements so labeled in Fig. 2.

It can be shown that the equations generated by minimization of H_n [equation (48)] with respect to the displacement components u_i, v_i and w_i [indicated in Fig. 1(b)] are the Euler equations of the variational problem in finite difference form. The equations corresponding to $\partial H_n/\partial u_i = 0$ and $\partial H_n/\partial v_i = 0$ represent equilibrium of in-plane forces at the stations where the u_i and v_i are specified; those corresponding to $\partial H_n/\partial w_i = 0$ represent equilibrium of normal forces at the stations where the w_i are specified.

Solution of the eigenvalue problem

The buckling loads or vibration frequencies are calculated from the set of linear, homogeneous, algebraic equations

$$[[K_1]+[K_2]+\Omega^2[M]]\{q\} = 0 \tag{48}$$

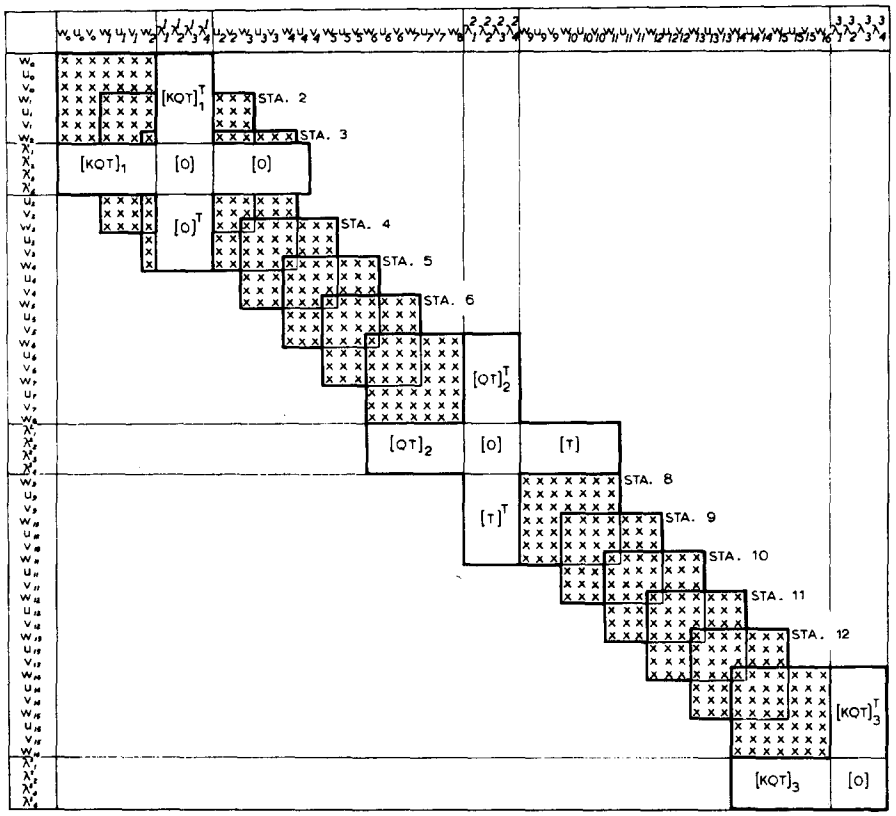

FIG. 2. Form of coefficient matrix with constraint conditions. This matrix corresponds to the model in Fig. 1(b).

for which non-trivial solutions exist if

$$|[K_1]+[K_2]+\Omega^2[M]| = 0. \tag{49}$$

The matrices $[K_1]$, $[K_2]$ and $[M]$ are strongly banded. In vibration problems for prestressed shells calculation of the lowest 5 or so eigenvalues is straightforward. A "classical" eigenvalue problem

$$[K_1+K_2]q+\Omega^2[M]q = 0 \tag{50}$$

is formulated, and the power method [17], [18] is used for calculation of the lowest few eigenvalues Ω^2 for a particular wave number n. The number of eigenvalues which can be determined accurately depends on the number of mesh points in the finite difference analysis and the complexity ("waviness" in the meridional direction) of the mode shapes.

In buckling problems the eigenvalues of $[K_1+K_2]$ for given n can be found by "plotting" $|K_1+K_2|$ versus the eigenvalue parameter λ ($\lambda \equiv p$, N_{10}, or other load) to obtain the load for which $|K_1+K_2|$ first vanishes. This technique was used in [4] for calculation of bifurcation loads of shells of revolution. On the other hand, a technique of successive approximation, similar to that employed by Cohen [2] for buckling problems can be used. This technique involves the definition of a sequence of "classical" eigenvalue problems which yields a sequence of loads that converges to the load for which $|K_1+K_2| = 0$. A typical

"classical" eigenvalue problem in the sequence is

$$[K_1+K_2]q+\lambda_k[K_2]q = 0. \tag{51}$$

Suppose the original load is p_1. The prestress terms N_{10}, N_{20}, N_{or} and χ_o which appear in $[K_2]$ are calculated for this load by means of the nonlinear analysis described in [12]. Then from equation (51) a value λ_1 is obtained. The new load is $p_2 = p_1(1+\lambda_1)$. New values of N_{10}, N_{20}, etc. corresponding to p_2 are now calculated from the nonlinear analysis of [12] and a new matrix $[K_2]$ is obtained. Then λ_2 is calculated from equation (51). The next value of the load is $p_3 = p_2(1+\lambda_2)$. The iteration process continues until λ_k, the kth correction, is smaller than some preassigned number. Convergence in some typical cases is discussed in the section on numerical results.

Truncation errors in modal stress resultants

Since a finite number of mesh points is used in the finite difference analysis, truncation errors occur. These errors are particularly large in the evaluation of the modal stress resultants at the boundaries of a shell and at the junctures between shell segments. In the absence of edge displacement constraint conditions and edge rings the natural boundary conditions $N_1 = 0$, $N_{12} = 0$, and $Q_1 = 0$ should be satisfied at the boundaries of the shell. The modal forces N_1, N_{12}, M_1 and Q_1 should be continuous at any juncture between shell segments, provided that the meridian and its slope are continuous and that no ring support exists here. It can be shown that such is the case in the limit $h \to 0$. The equations which correspond to three of the natural boundary conditions at the end "A" of the shell are $\partial H_n/\partial u_o = 0$, $\partial H_n/\partial v_o = 0$, and $\partial H_n/\partial w_o = 0$ (see Figs. 1 and 2). These equations yield, respectively:

$$N_1+\Delta N_1 = 0, \qquad N_{12}+\Delta N_{12} = 0, \qquad M_1+\Delta M_1 = 0 \tag{52}$$

where ΔN_1, ΔN_{12} and ΔM_1 are the truncation errors and are given approximately by:

$$\begin{aligned}
\Delta N_1 &= -\frac{h}{2r}(N_2 r' + N_{12} n - N_{10}\chi r/R_1)_A, \\
\Delta N_{12} &= +\frac{h}{2r}(N_{12} r' + N_2 n + N_{20}\psi r/R_2)_A, \\
\Delta M_1 &= -\frac{h}{2r}(M_2 r' - M_t n + N_1\chi_o r + N_{10}\chi r)_A.
\end{aligned} \tag{53}$$

The quantities ΔN_1, ΔN_{12} and ΔM_1 for the end "B" of the shell are given by equation (53) with the opposite signs. For a shell of many segments, equations (53) apply at the ends of each segment, even if rings are present at the junctures between segments. Errors in the modal stresses N_2 and M_2 at the ends of segments are given approximately by:

$$\begin{aligned}
\Delta N_2 &= C_{12}\Delta N_1/C_{11} \\
\Delta M_2 &= C_{45}\Delta M_1/C_{44}.
\end{aligned} \tag{54}$$

Figure 3 shows the discontinuities in modal stresses occurring between segments of shells. The top three plots give N_1, N_2 and N_{12} for the buckling mode of a shallow spherical cap with an edge ring. The bottom plot gives M_1 for the fundamental vibration mode of a

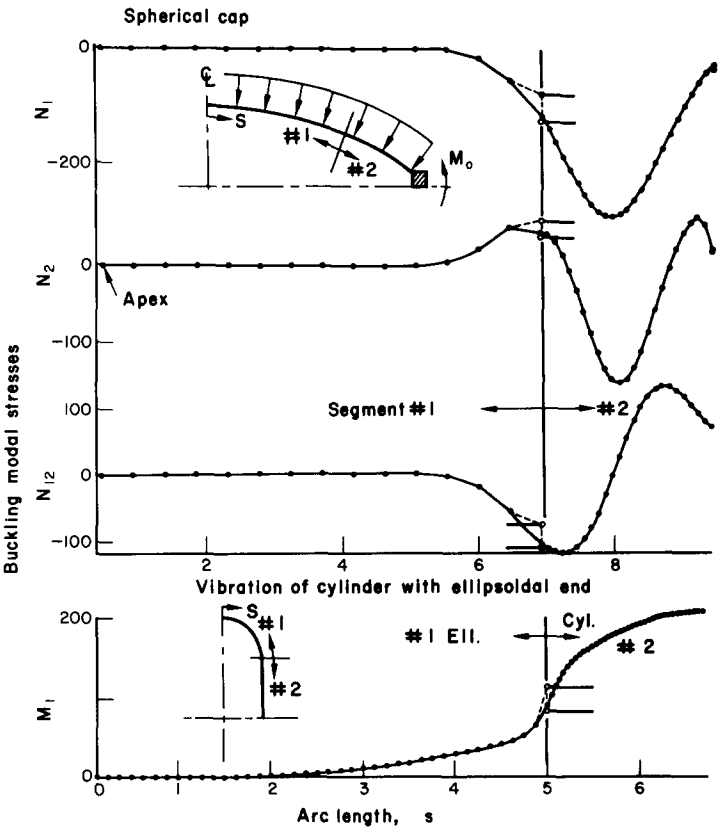

FIG. 3. Buckling and vibration modal stress resultants showing local truncation errors.

cylinder with an ellipsoidal end closure. The circles at the juncture represent the stresses calculated by use of equations (5) and (6)–(9) without correction for the errors ΔN_1, ΔN_2, ΔN_{12} and ΔM_1. Subtraction of the errors (53) and (54) results in modal stresses which are continuous at the juncture. It is evident from Fig. 3 that these errors at the juncture and edge do not "propagate" into the adjacent shell segments. Similar results have been obtained at the boundaries of shells with partially free edges (e.g. simply-supported).

Correction of the modal stresses at shell edges and junctures does not affect the eigenvalues, and is therefore not of great significance in buckling and vibration analyses. However, such corrections would have to be made in the finite difference stress analysis of shells. Similar behavior is expected, for example, in the stress analysis of non-symmetrically loaded shells by a two-dimensional finite difference scheme. Since the edge stresses are likely to be the largest, it is important to calculate them as accurately as possible.

NUMERICAL RESULTS

The computer program based on the nonlinear stress analysis of [12] and the linear stability and vibration analysis presented above has been checked through cases for which solutions are known. A rather extensive investigation has been performed of the convergence

properties of the eigenvalues with respect to number of points in the finite difference mesh and with respect to number of iterations required for the solution of nonlinear problems. Additional numerical results, including comparisons between test and theory, are given in [13].

Convergence properties

Table 1 gives six examples of the convergence of the sequence of eigenvalue problems as defined by equation (51). The first two examples are for an externally pressurized spherical cap with an edge ring and a constant applied edge moment, M_O (see top of Fig. 3 for geometry). The zeroth iteration represents the program user's initial guess of the critical load. In Example 1 the convergence criterion for the pressure (0·1 %) is satisfied after four iterations. Example 2 represents a problem in which nonlinear effects are dominant because of the large edge moment $M_O = 0{\cdot}8$ in-lb/in., applied to the spherical cap. Convergence of the pressure is rather slow, and calculations are terminated before the solution has con-

TABLE 1. CONVERGENCE OF SEQUENCE OF EIGENVALUE PROBLEMS $[K_1 + K_2]\{q\} + \lambda_k[K_2]\{q\} = 0$

Iteration number k	Ex. 1† Sph. cap $M_o = 0{\cdot}2$ p_{cr} (psi)	Ex. 2 Sph. cap $M_o = 0{\cdot}8$ p_{cr} (psi)	Ex. 3 Cyl. (Fig. 4) 11 points N_{cr} (lb/in.)	Ex. 4 Cyl. (Fig. 4) 41 points N_{cr} (lb/in.)	Ex. 5 Cyl. (Fig. 4) 91 points N_{cr} (lb/in.)	Ex. 6 Cyl. (Fig. 4) 91 pts. D.P. N_{cr} (lb/in.)
0	0·20000	0·1000	7750·0	7750·0	7750·0	7750·0
1	0·65002	0·1407	7960·0	7766·3	7917·8	7775·5
2	0·78577	0·1927	8021·9	7777·7	8098·0	7784·0
3	0·77928	0·2546	8039·6	7781·5	8247·0	7786·8
4	0·77965	0·3221	8044·6	7782·5	8103·4	7787·8
5		0·3883	8046·0	7778·4	8128·1	7788·1
6		0·4462	8046·4	7771·2	8135·2	
7		0·4917		7779·6	8216·1	
8		0·5245		7781·4	8260·4	
9		0·5466			8192·8	
10		0·5609			8009·8	
11		0·5699			8257·6	

† Ex. 1 and 2 are for externally pressurized spherical caps with edge rings (see Fig. 3, top). Ex. 3–6 are for axially compressed, longitudinally stiffened cylinders (see Fig. 4). Ex. 6 calculations in double precision.

verged to the required accuracy of 0·1 %. With a better initial guess for p_{cr} or if iterations are allowed to continue, a solution of $p_{cr} = 0{\cdot}582$ psi is obtained. Examples 3–6 all apply to the same axially compressed cylindrical shell for which various numbers of mesh points are used (see Fig. 4 for geometry). The first three examples give results from single-precision calculations and the last example gives results from double-precision calculations. The accuracy required for computer "approval" of the solution is 0·01 %. It is seen that round-off errors cause some difficulty in Example 4 and prevent completely convergence in Example 5. It is also clear from Example 5 that a convergence criterion could be chosen (such as 1 %) which would lead to "approval" of the solution 8135·2 lb-in. This load is not within 1 % of the correct load (7788·1 lb/in.). It is evident from the double-precision calculations of Example 6, that round-off errors cause the discrepancy. Figure 4 shows how round-off errors can lead to erroneous results when calculations are performed in single precision. The loads corresponding to 41 and 51 mesh points are "converged" solutions in

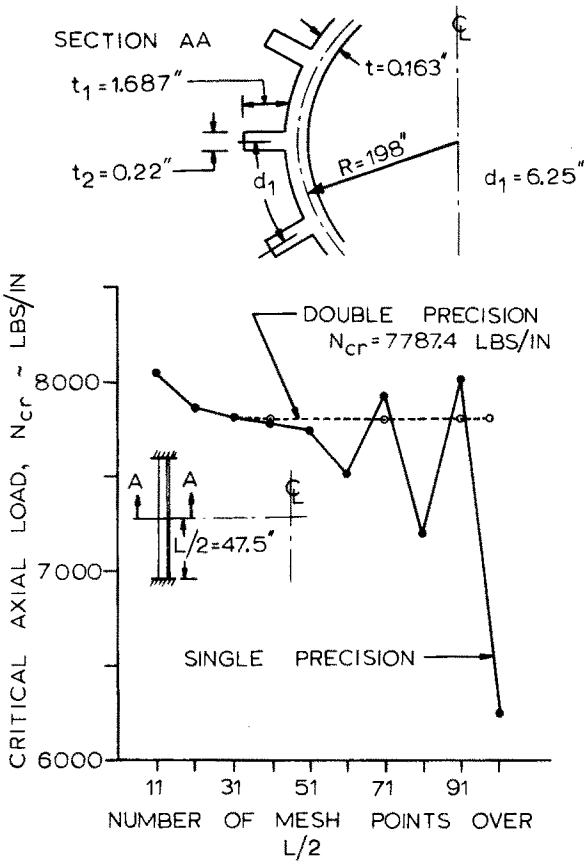

FIG. 4. Convergence of buckling load with increase in number of mesh points.

the sense of Table 1, but they do not have the required accuracy when compared with the solutions labeled "Double Precision". Further increase in the number of mesh points with single-precision calculations leads to further deterioration in the accuracy of the results.

Table 2 gives buckling loads for a spherical shell with an edge angle $\alpha = 160°$ and a free edge. The wave number $n = 2$. Loads are tabulated as a function of the number and the distribution of mesh points. Run times for the Univac 1108 digital computer are also given. These are the times in seconds required for calculation of the buckling load for a single value of the wave number n. Nonlinear prebuckling effects are included. It is seen that much accuracy is gained in this case by division of the shell into two segments. Mesh points are concentrated in the edge region where the modal displacements vary rapidly. For two cases double-precision calculations were made as a check on the single-precision results.

Figure 5 shows a cylindrical shell stiffened by small and large rings. It is desired to find the buckling pressure of this shell. In the analysis the small rings are "smeared out" (see [16]) and the intermittant large rings are treated as discrete elastic structures. The large rings cause significant local disturbances in the prebuckling and buckling modal behavior, as seen in Fig. 6. It is therefore advantageous to analyze the single shell in segments, concentrating mesh points near the large rings where prebuckling and buckling modal displacements vary rapidly.

TABLE 2. BUCKLING LOADS OF A SPHERICAL SHELL, $\alpha = 160°$, $A = 0$, $E = 0{\cdot}91$, $\nu = 0{\cdot}3$ CONVERGENCE WITH NUMBER AND DISTRIBUTION OF MESH POINTS; COMPUTER TIME

Number of mesh points	How distributed	Buckling pressure $p_{cr} \times 10^7$ (lb/in^2) single precision	Buckling pressure $p_{cr} \times 10^7$ (lb/in^2) double precision	Univac 1108 computer time (seconds) single precision
30	1 Segment	19·345		8·511
40	1 Segment	26·978		10·235
50	1 Segment	30·730		10·186
60	1 Segment	32·650		11·794
70	1 Segment	33·761		10·411
80	1 Segment	34·417		11·847
90	1 Segment	34·866		9·614
97	1 Segment	35·056		10·069
10, 10	2 Segments (0°–135°) (135°–160°)	33·594		4·574
15, 15	2 Segments (0°–135°) (135°–160°)	35·405		5·626
20, 20	2 Segments (0°–135°) (135°–160°)	35·872		6·946
25, 25	2 Segments (0°–135°) (135°–160°)	36·039		8·595
30, 30	2 Segments (0°–135°) (135°–160°)	36·090		9·434
35, 35	2 Segments (0°–135°) (135°–160°)	36·160	36·175	10·670
40, 40	2 Segments (0°–135°) (135°–160°)	36·157		11·981
45, 45	2 Segments (0°–135°) (135°–160°)	36·206	36·223	13·223
	double			

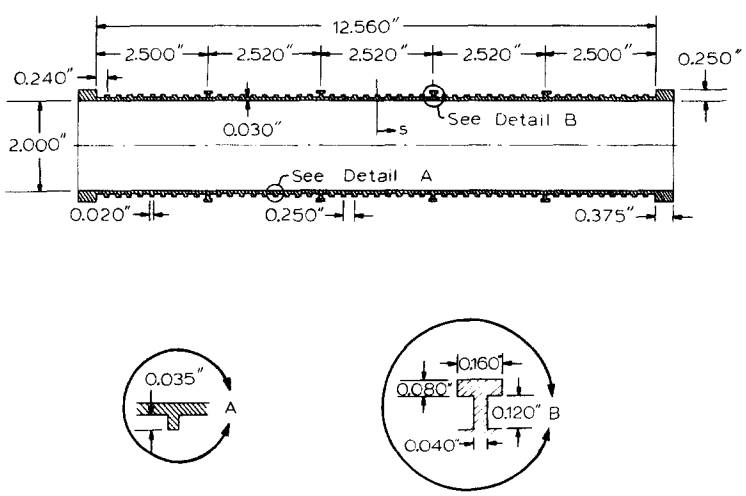

FIG. 5. Geometry of ring-stiffened cylinder submitted to external hydrostatic pressure.

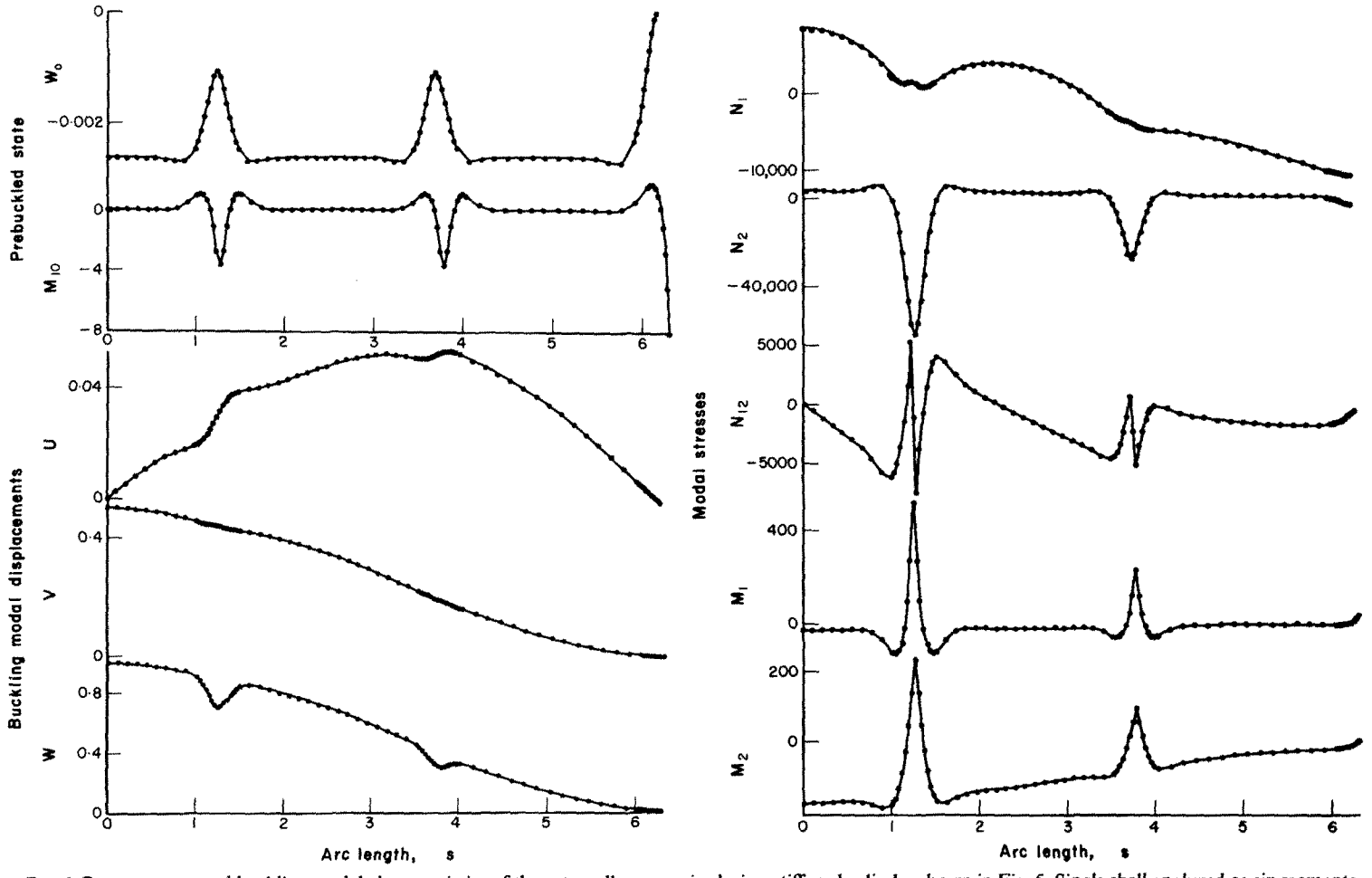

FIG. 6. Prestress state and buckling modal characteristics of the externally pressurized, ring-stiffened cylinder shown in Fig. 5. Single shell analyzed as six segments with mesh points concentrated around large rings.

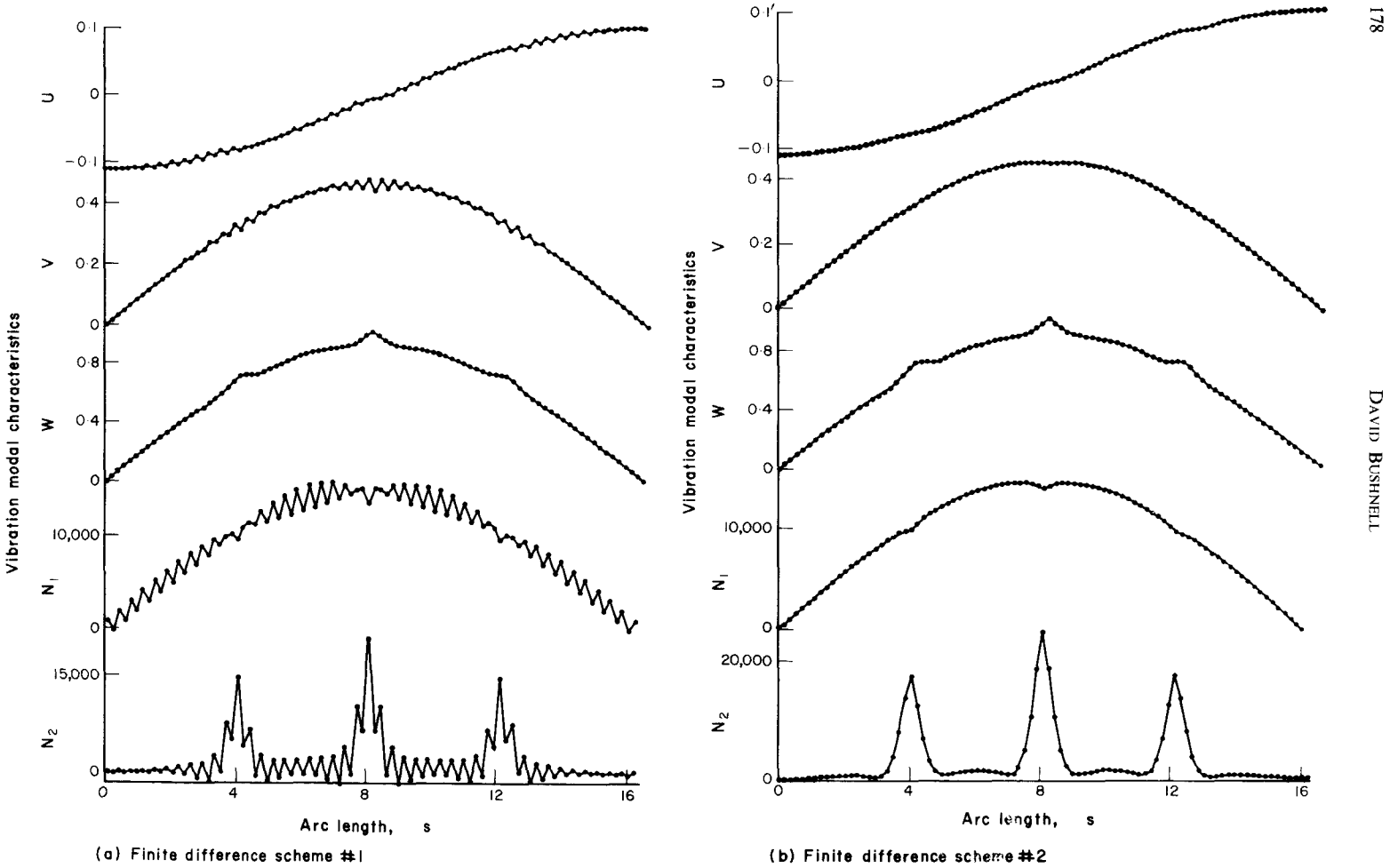

FIG. 7. Comparison of vibration modal characteristics with finite-difference schemes No. 1 and No. 2 for the ring-stiffened cylinder shown in Fig. 9.

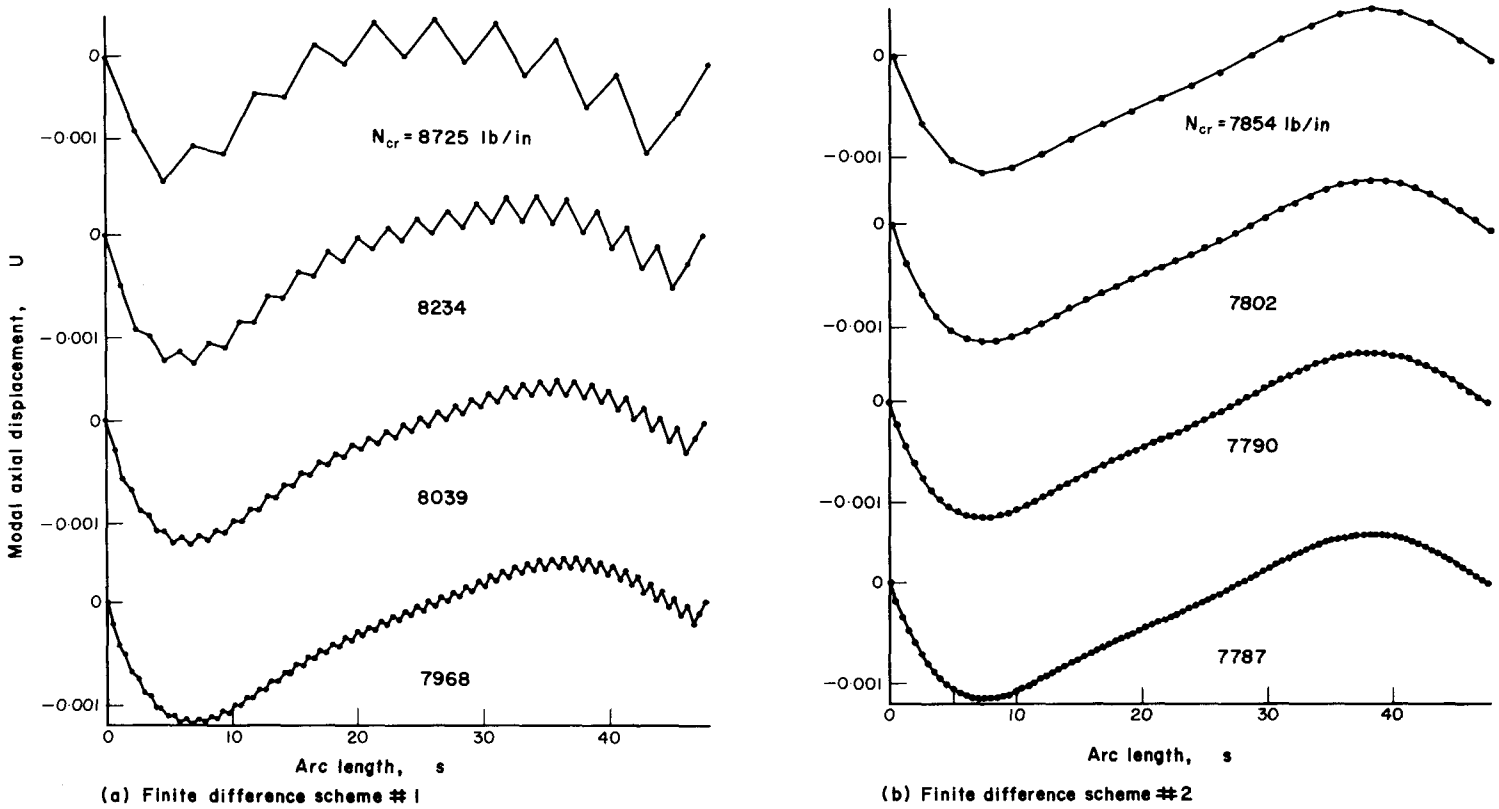

FIG. 8. Comparison of buckling modal displacement u with finite-difference Schemes No. 1 and No. 2 for the axially compressed cylinder shown in Fig. 4.

Comparison of two finite difference schemes

Figures 7 and 8 show comparisons between a finite-difference scheme in which all the displacement components u_i, v_i and w_i are specified at the same point (Scheme #1) and the scheme indicated in Fig. 1(b) and equations (9) (Scheme #2). In the Scheme #1 central differences are used everywhere except at the ends "*A*" and "*B*" of the shell, where forward and backward differences are used, respectively. With Scheme #1 the coupling between adjacent u_i and v_i values is weak, since no second derivatives of these variables appear in the energy expression. This situation often leads to the "jumpy" behavior of the eigenvector and affects the accuracy of the eigenvalue. Figure 7 shows the fundamental vibration mode of a ring-stiffened cylinder as calculated by the two schemes. The cylinder and ring geometry are shown in Fig. 9. Figure 8 shows the buckling modal displacement u of the axially compressed cylinder depicted in Fig. 4. Convergence of the critical load with number of mesh points is far more rapid with the finite-difference Scheme #2 than with Scheme #1.

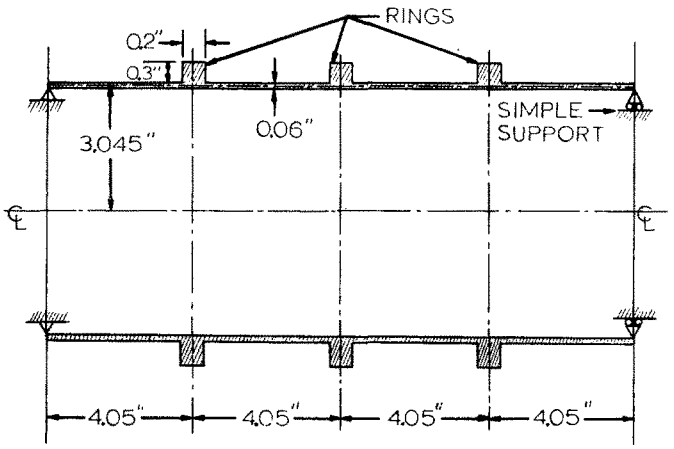

FIG. 9. Geometry of vibrating ring-stiffened cylinder.

REFERENCES

[1] G. A. COHEN, Computer analysis of asymmetric free vibrations of ring-stiffened orthotropic shells of revolution. *AIAA Jnl.* **3**, 2305 (1965).
[2] G. A. COHEN, Computer analysis of asymmetric buckling of ring-stiffened orthotropic shells of revolution. *AIAA Jnl.* **6**, 141 (1968).
[3] A. KALNINS, Analysis of shells of revolution subjected to symmetrical and nonsymmetrical loads. *J. appl. Mech.* 467 (1964).
[4] B. O. ALMROTH and D. BUSHNELL, Computer analysis of various shells of revolution. Presented AIAA 6th Aerospace Sciences Meeting, New York, Jan. 1968, *AIAA Jnl.* **6**, 1848 (1968).
[5] E. REISSNER, On axisymmetrical deformation of thin shells of revolution. *Proc. of Symposia in Applied Mathematics*, Vol. III, p. 27. McGraw-Hill (1950).
[6] V. V. NOVOSHILOV, *The Theory of Thin Shells*, Chapter 1, pp. 18 and 24. Noordhoff (1959).
[7] H. WEINITSCHKE, On the stability problem for shallow spherical shells. *J. Math. Phys.* **38**, 209 (1960).
[8] B. BUDIANSKY, Buckling of clamped shallow spherical shells. *Proc. IUTAM Symp. of Theory of Thin Elastic Shells*, p. 64. North-Holland (1960).
[9] M. STEIN, The effect on the buckling of perfect cylinders of prebuckling deformations and stresses induced by edge support. Collected Papers on Instability of Shell Structures, NASA TN D-1510, p. 217 (1962).
[10] N-C. HUANG, Unsymmetrical buckling of thin shallow spherical shells. *J. appl. Mech.* **31**, 447 (1964).

[11] C. STUHLMAN, A. DELUZIO and B. ALMROTH, Influence of stiffener eccentricity and end moment on stability of cylinders in compression. *AIAA Jnl.* **4**, 872 (1966).
[12] D. BUSHNELL, Nonlinear analysis for axisymmetric elastic stresses in ring-stiffened, segmented shells of revolution. Proceedings ASME/AIAA 10th Structures, Structural Dynamics & Materials Conference, New Orleans, pp. 104–113 (1969).
[13] D. BUSHNELL, Buckling and vibration of ring-stiffened, segmented shells of revolution, Part 2, Numerical results. *Proc. First International Piping and Pressure Vessel Technology Conference*, Delft (1969).
[14] G. A. COHEN, Buckling of axially compressed cylindrical shells with ring-stiffened edges. *AIAA Jnl.* **4**, 1859 (1966).
[15] G. A. COHEN, Conservativeness of a normal pressure field acting on a shell. *AIAA Jnl.* **4**, 1886 (1966).
[16] D. BUSHNELL, B. O. ALMROTH and L. H. SOBEL, Buckling of shells of revolution with various wall constructions, Vol. 2—Basic equations and method of solution. NASA CR-1050 (May 1968).
[17] F. BODEWIG, *Matrix Calculus*. North-Holland (1959).
[18] E. Y. TSUI, F. A. BORGAN and P. STERN, Juncture stress fields in multicellular structures. Lockheed Missiles and Space Co. Report M-77-65-5, Vol. 1 (1965).

(*Received* 8 *November* 1968; *revised* 8 *May* 1969)

Абстракт—Используется энергическая формулировка вместе с методом конечных разностей, с целью выведения уравнений, приводящих к нагрузкам выщучивания и частотам колебаний сегментных упругих оболочек вращения, поддержанных кольцами. Кольца рассматриваются как дискретные упругие конструкции. Дается квадраткая форма для полной потенциальной и кинетической энергии, путем интенсивного применения матричных методов. Разработка оказывается подобна к той, которая используется в методе конечного элемента. Она идеально подходит для программировки на вычислительные машины. Дается численные результаты, в которых сравниваются два типа приближений в конечных разностях. Исследуются свойства сходимости собственных значений и собственных векторов.